TEMPERATURE-DEPENDENT FORMATION OF OZONE IN SOLID OXYGEN BY 5 keV ELECTRON IRRADIATION AND IMPLICATIONS FOR SOLAR SYSTEM ICES

Bhalamurugan Sivaraman,[1] Corey S. Jamieson,[2] Nigel J. Mason,[1] and Ralf I. Kaiser[1,2]
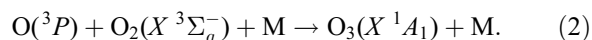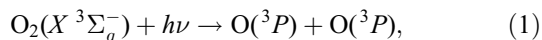
ABSTRACT

We have investigated the formation of ozone by electron impact in solid molecular oxygen ices between 11 and 30 K. The amount of ozone formed is shown to be strongly dependent on the sample temperature. As the ice temperature increases, the column density of the ozone monomer is found to diminish. This is ascribed to the loss of oxygen atoms by recombination with a neighboring oxygen atom to "recycle" molecular oxygen. In the "warm-up" phase after irradiation, two additional temperature-dependent reaction mechanisms were observed to synthesize ozone: (1) a reaction of oxygen atoms from a $[O_3...O]$ complex with a neighboring oxygen molecule and (2) a reaction of trapped oxygen atoms with oxygen molecules to yield the ozone monomer. These experiments have important implications to the oxygen chemistry in icy satellites throughout our solar system.

Subject headings: astrochemistry — ISM: molecules — methods: laboratory — molecular processes — planets and satellites: general

Online material: color figures

1. INTRODUCTION

Ozone is believed to be an essential component of any planetary atmosphere capable of sustaining life; hence, the detection of ozone in the atmosphere of exoplanets is a major objective of both the *Darwin* and *Terrestrial Planet Finder* (*TPF*) space telescopes (Beichman et al. 1999; Leger 2000). The observation of an exoplanetary atmosphere containing water, oxygen, carbon dioxide, and ozone would then be regarded as strong evidence that the planet can support life, perhaps even providing strong circumstantial evidence of the existence of life itself (Angel et al. 1986; Burke 1986; Leger et al. 1994, 1999). On Earth, the development of an oxygen-rich atmosphere is attributed to developing photosynthesis from ocean-based plants like algae (Berkner & Marshall 1964). Eventually, concentrations of molecular oxygen in the atmosphere were sufficiently high to allow the development of a stratospheric ozone layer by the well-known Chapman reactions (1) and (2) (Chapman 1930),

$$O_2(X\ ^3\Sigma_g^-) + h\nu \rightarrow O(^3P) + O(^3P), \tag{1}$$

$$O(^3P) + O_2(X\ ^3\Sigma_g^-) + M \rightarrow O_3(X\ ^1A_1) + M. \tag{2}$$

Ozone is created when solar ultraviolet (UV) radiation ($\lambda <$ 240 nm) dissociates oxygen molecules to form atomic oxygen, which quickly combines with other oxygen molecules to form ozone via a three-body collision. The formation of a stratospheric ozone layer that was thick enough to filter UVA and UVB from the terrestrial surface in turn led to the development of land-based flora and eventually fauna. This simple description of evolution is supported by fossil evidence and, therefore not surprisingly, has been adopted as a generalized mechanism for the evolution of life on other planetary bodies. This in turn has led to the continued support for ozone as an essential biomarker of any habitable world.

The first tentative evidence for the presence of ozone on an extraterrestrial planetary body was provided by the *Mariner 7* spacecraft (Barth & Hord 1971), which revealed ozone in the Martian atmosphere. Subsequent extensive studies by the *Mariner 9* spacecraft revealed seasonal abundance variations (Barth et al. 1973). These observations were explained by photolysis of carbon dioxide (CO_2) liberating oxygen atoms, which subsequently formed oxygen and ultimately ozone via the Chapman mechanism. The arrival of the *Mars Express* with SPICAM has provided additional information on ozone in the Martian atmosphere (Bertaux et al. 2000). The first suggestion of ozone being formed on a planetary moon was provided by the *International Ultraviolet Explorer* (*IUE*; Nelson et al. 1987), which suggested the presence of ozone on the surface of Ganymede. This was confirmed by Noll et al. (1996) using the *Hubble Space Telescope* (*HST*) Faint Object Spectrograph; the authors report the observation of an absorption feature at 260 nm, a feature they ascribed to the Hartley continuum of ozone. *Galileo* Ultraviolet Spectrometer (UVS) spectra confirmed the findings and provided the first map of ozone on the surface of Ganymede (Hendrix et al. 1999). Noll et al. (1997) used the Space Telescope Imaging Spectrograph (STIS) on *HST* to make available global disk-resolved maps of the 260 nm absorption band; this map revealed that the absorption was stronger in the trailing hemisphere. These results were initially controversial, since it was not thought possible that ozone could be formed in any atmosphere/ice that was not oxygen-rich. However, Noll et al. (1997) reported similar spectroscopic features in the absorption spectra of the Saturnian moons Rhea and Dione. The identification of ozone on moons around two different planets in regions of the solar system with quite distinct solar fluxes and quite different planetary compositions removed the possibility that there were special circumstances unique to Ganymede. Consequently, the process of ozone formation in the water ice–covered moons was apparently more general and not biological in origin; thus, ozone could not after all be regarded as a unique biomarker.

But what are the mechanisms for ozone formation on these bodies whose temperatures are in the range 70–150 K? (Bertaux et al. 2000; Hanel et al. 1979, 1982; Spencer et al. 1999.) Since Ganymede, Rhea, and Dione are too small to support an atmosphere, the formation of ozone by photolysis in the atmosphere is

[1] Department of Physics and Astronomy, The Open University, Walton Hall, Milton Keynes, MK7 6AA, United Kingdom; n.j.mason@open.ac.uk.

[2] Department of Chemistry, University of Hawaii at Manoa, Honolulu, HI 96822; ralfk@hawaii.edu.
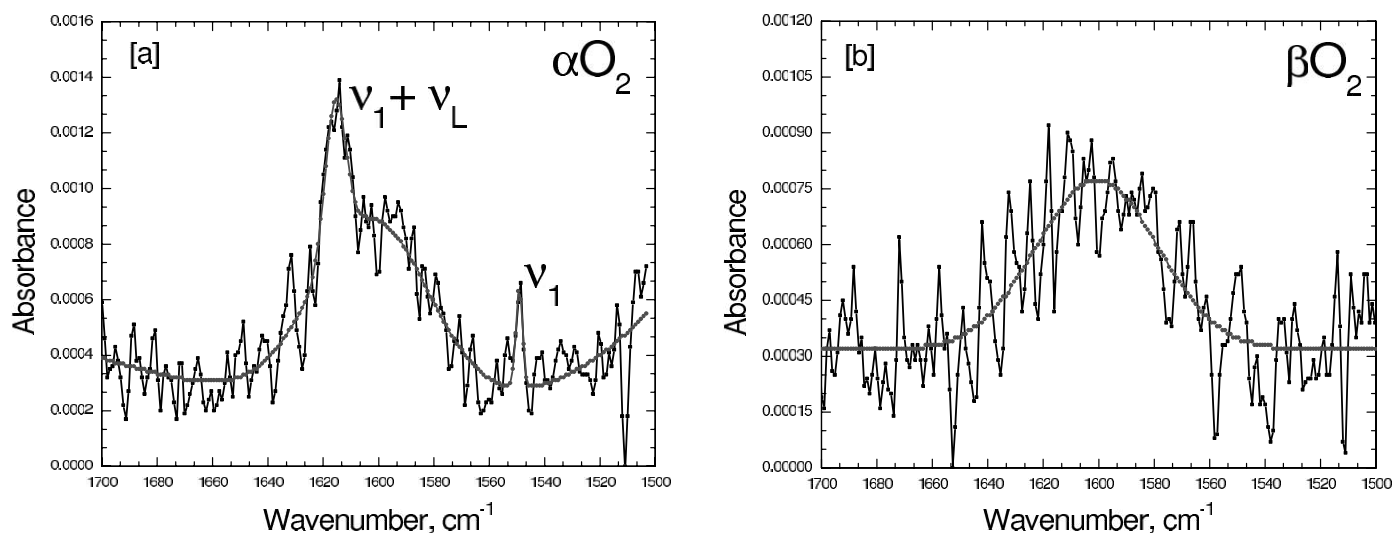
Fig. 1.—Matrix-induced infrared band of solid O_2 in the α and β phases. (a) Solid oxygen deposited at 11 K is identified as α-O_2 via its infrared bands observed at 1549 cm^{-1} (ν_1) and 1614 cm^{-1} ($\nu_1 + \nu_L$). (b) Sample was warmed up to 30 K at the rate of 0.5 K minute^{-1}; the solid oxygen phase is identified to be β-O_2 (1595 cm^{-1}). [See the electronic edition of the Journal for a color version of this figure.]

not feasible; therefore, an alternative formation process is required to explain the astronomical observations. Since all three moons lie within the magnetosphere of their planetary parent bodies, it was proposed that the ozone is formed by charged particles penetrating the icy, water-rich surface of the moon, thus triggering nonequilibrium chemistry (Teolis et al. 2006). However, very little information exists on the precise mechanisms involved in the *temperature-dependent* formation of ozone in astrophysically relevant ices. Baragiola et al. (1999) and Fama et al. (2002) have investigated the ozone formation in 100 keV proton–irradiated oxygen matrices; Lacombe et al. (1997), using low-energy (up to 10 eV) electrons, and Bennett & Kaiser (2005), using 5 keV electrons, have unraveled the mechanisms that form ozone using electron irradiation of molecular oxygen ices at 10 K. In this paper, we investigate the temperature-dependent formation mechanisms of ozone and report the yields together with the production rates of ozone as a function of ice temperature (11–30 K) and electron beam current. These data will help us to predict the existence of ozone on solar system bodies quantitatively.

2. EXPERIMENTAL

The present experiments were carried out in a contamination-free ultra–high-vacuum stainless steel chamber (Bennett & Kaiser 2005). The chamber can reach pressures down to 5×10^{-11} torr by use of a magnetically suspended turbomolecular pump that is backed by a scroll pump. All pumps used are oil free to ensure no hydrocarbon contaminants enter the system. Temperatures down to 11 K are reached using a two-stage closed-cycle helium refrigerator that is interfaced directly to a polished single-crystal silver mirror onto which the ices are condensed. The silver substrate is suspended by a differentially pumped rotatable feedthrough, which aligns the substrate in the center of the main chamber. Gas is deposited onto the substrate at 11 K, with the gas flow regulated by a thermovalve that introduces the gas through the linear transfer mechanism to a gas capillary array which evenly disperses the gas. Molecular oxygen (99.99%, Gaspro) was condensed for 300 s at a pressure of 10^{-7} torr at 11 K. To prepare the 20 and 30 K oxygen ice samples, the gases were first condensed at 11 K followed by a slow heating of the ice samples at a rate of 0.5 K minute^{-1} to the desired temperature. The sample thicknesses were 300 ± 30 nm (11 K), 275 ± 30 nm (20 K), and 130 ± 15 nm (30 K).

The ice samples were irradiated isothermally with 5 keV electrons to cleave the oxygen-oxygen bond. The electron beam was operated at a nominal current of 100 nA with an extraction efficiency of 78.8% and scanned over the sample area 1.8 ± 0.3 cm^2 to avoid heating the ice. Note that these energetic electrons simulate the processes occurring in the track of galactic cosmic-ray protons and helium nuclei (Holtom et al. 2005); in addition, keV electrons are trapped in the magnetospheres of the giant planets like Jupiter and Saturn which can interact with the water-rich surface of their satellites. The samples were irradiated for 1 hour, which exposed the target to 1.8×10^{16} electrons. The reactions were monitored using a Nicolet 510 DX Fourier Transform Infrared Spectrometer (FTIR). The spectrometer has a wavenumber range of 6000–500 cm^{-1} and operates in absorption-reflection-absorption mode with a reflection angle of 75° from the normal relative to the mirror surface. Infrared spectra of the ice were recorded online and in situ at an integrated time of 2.5 minutes and at a resolution of 2 cm^{-1}. The column densities of a molecule can be calculated according to Bennett & Kaiser (2005). After the irradiation, the sample was left isothermally for 1 hour and was then slowly warmed at the rate of 0.5 K minute^{-1}. The sublimation of the molecules into the gas phase was monitored by a quadrupole mass spectrometer (1–200 amu).

3. RESULTS

3.1. *Infrared Spectra*

After depositing molecular oxygen at 11 K, an infrared band in the ice was observed at 1549 cm^{-1}, which can be assigned to the O—O stretching of the ν_1 fundamental (Fig. 1a; Freiman & Jodl 2004). At 1614 cm^{-1}, we also detected a broad absorption band which is attributed to a combination band of the ν_1 fundamental and the translational lattice mode (ν_L). It should be noted that solid molecular oxygen exists in three different crystalline phases (Cairns & Pimentel 1965). These are α-O_2 between 0 and 23.9 K (monoclinic phase; Barrett et al. 1967), β-O_2 between 23.9 and 43.6 K (rhombohedral; Horl 1962), and γ-O_2 between 43.6 and 54.4 K (Horl 1962). Under ultra–high-vacuum (UHV) conditions, molecular oxygen ice starts to sublime at about 30 K, and most of the oxygen matrix is lost between 36 and 42 K; therefore, in the present studies, only α-O_2 and β-O_2 are likely to be important.

FIG. 2.—Deconvolution of the ν_3 band of ozone at 11 K (*top*), 20 K (*center*), and 30 K (*bottom*). [*See the electronic edition of the Journal for a color version of this figure.*]
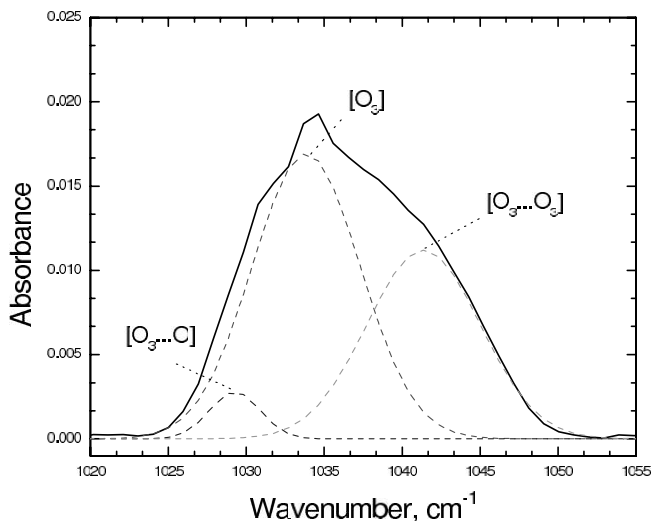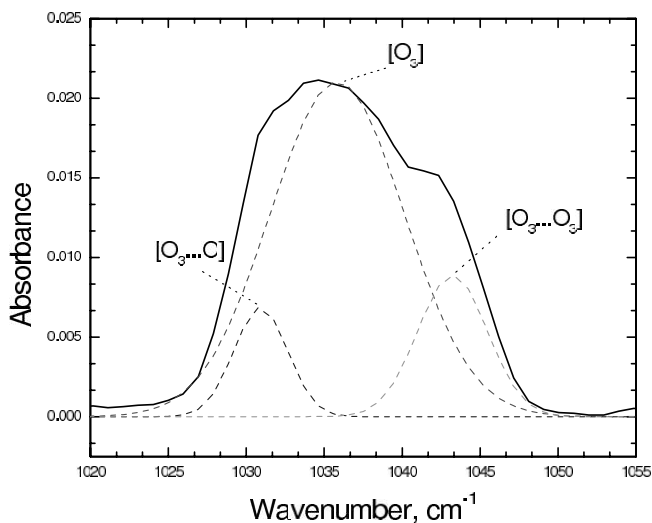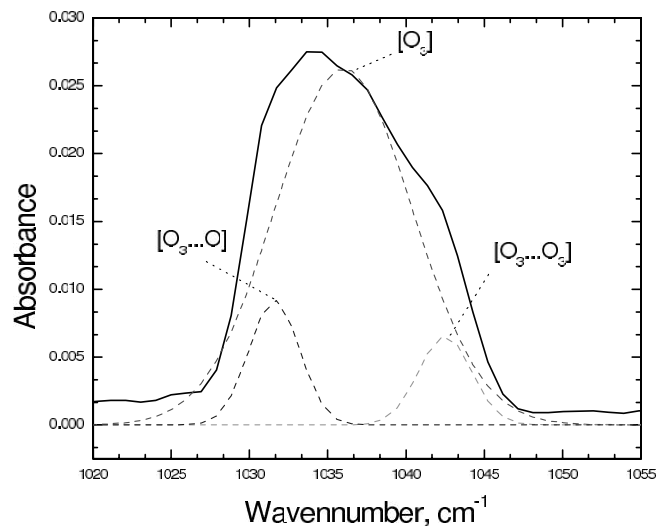
TABLE 1
INFRARED ABSORPTION BANDS OF OZONE OBSERVED
IN THE SAMPLE IRRADIATED AT 11 K

MODE	WAVENUMBER AT $T=$ (cm^{-1})		WAVENUMBER FROM THIS WORK (cm^{-1})		CHARACTERIZATION
	5 K[a]	10 K[b]	α-O$_3$[c]	β-O$_3$	
ν_1	1108.8	1103.5	1104	1107	O—O symmetric stretch
ν_2	703.9	708.5	702	708.7	O—O—O bend
ν_3	1037	1037	1037	1036[d]	O—O asymmetric stretch
$2\nu_3$	2045.3	2047	2044	2048.5	Overtone
$3\nu_3$	3033.6	3035	3028	3033.5	Overtone
$2\nu_1$	2210	...	...	...	Overtone
$\nu_1 + \nu_2$	1803.9	...	...	...	Combination band
$\nu_1 + \nu_3$	2108.1	2105	2105	2108.6	Combination band
$\nu_2 + \nu_3$	1723.8	1720	1721	1725	Combination band
$\nu_2 + 3\nu_3$	3703.9	...	...	...	Combination band
$\nu_1 + \nu_2 + \nu_3$	2787.1	2800	2798	...	Combination band

[a] Absorption frequencies of the O$_3$ monomer taken from Brosset et al. (1993).
[b] Absorption frequencies of the O$_3$ monomer taken from Brewer & Wang (1972).
[c] Absorption frequencies of the O$_3$ monomer in good agreement with Bennett & Kaiser (2005).
[d] Absorption frequency of the O$_3$ monomer that did not match with the previous value obtained by Chaabouni et al. (2000b).

The infrared spectra of solid oxygen depends strongly on the phase. By comparing our infrared spectra with previous studies (Smith et al. 1950), we can therefore assign the phase of the molecular oxygen in our experiments. Our infrared spectra suggest the existence of α-O$_2$ at 11 K (Fig. 1a) and β-O$_2$ at 30 K (Fig. 1b).

With the onset of electron irradiation, additional absorption features appeared in our infrared spectra (Fig. 2). These could be attributed to the ozone molecule (O$_3$). Out of 11 infrared bands reported by Brosset et al. (1993) in a study of solid ozone film deposited at 5 K, we observed seven new bands in our oxygen film after irradiation at 11 K (Table 1). These are ν_1 (1104 cm^{-1}), ν_2 (702 cm^{-1}), ν_3 (1037 cm^{-1}), $2\nu_3$ (2044 cm^{-1}), $3\nu_3$ (3028 cm^{-1}), $\nu_2 + \nu_3$ (1721 cm^{-1}), and $\nu_1 + \nu_3$ (2105 cm^{-1}). The positions and relative intensities of all bands are in excellent agreement with those reported in earlier studies (Bennett & Kaiser 2005; Brewer & Wang 1972; Dyer et al. 1997; Schrivermazzuoli et al. 1995). The $\nu_1 + \nu_2 + \nu_3$ band (2798 cm^{-1}) was also observed during the warm-up phase (Bennett & Kaiser 2005).

A detailed inspection of the profile of the ν_3 band suggests that this feature is in fact a composite structure (Fig. 2). A deconvolution reveals three different features: one due to the ozone monomer at 1037 cm^{-1} and two close satellite peaks at 1032 and 1042 cm^{-1}; the first attributable is to the ozone-oxygen complex [O$_3$...O], whereas the latter can be assigned to the ozone dimer [O$_3$...O$_3$] (Bahou et al. 2001; Bennett & Kaiser 2005; Chaabouni et al. 2000b; Schrivermazzuoli, et al. 1995). The [O$_3$...O] complex was observed about 200 s after the onset of irradiation. The formation of the ozone dimer, [O$_3$...O$_3$], is only detectable at longer irradiation times of 1500 s.

When the irradiated sample was slowly warmed, new bands are observed in the ice spectra above 47 K, after the molecular oxygen has completely sublimed (Fig. 3). The 1049 cm^{-1} feature, which appears above 47 K, resides close to the ozone dimer and can be assigned to the formation of ozone clusters, (O$_3$)$_n$ (Chaabouni et al. 2000a, 2000b). The ν_1, ν_2, and $\nu_1 + \nu_3$ combination bands are observed at 1107, 709, and 2108 cm^{-1}, respectively. These assignments are in good agreement with a previous study carried
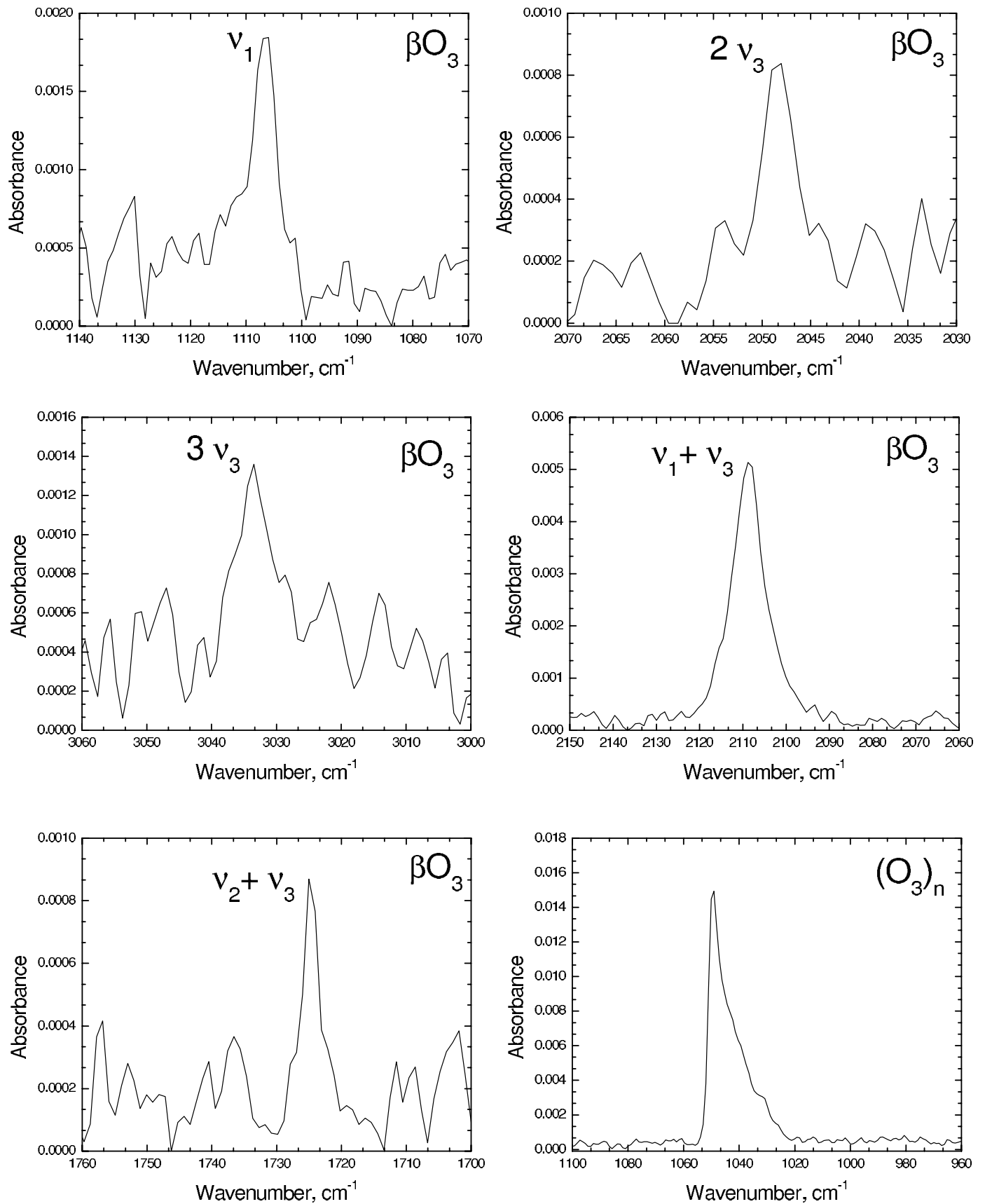
FIG. 3.—Observed infrared absorption bands during the warm-up of the irradiated sample to 47 K.
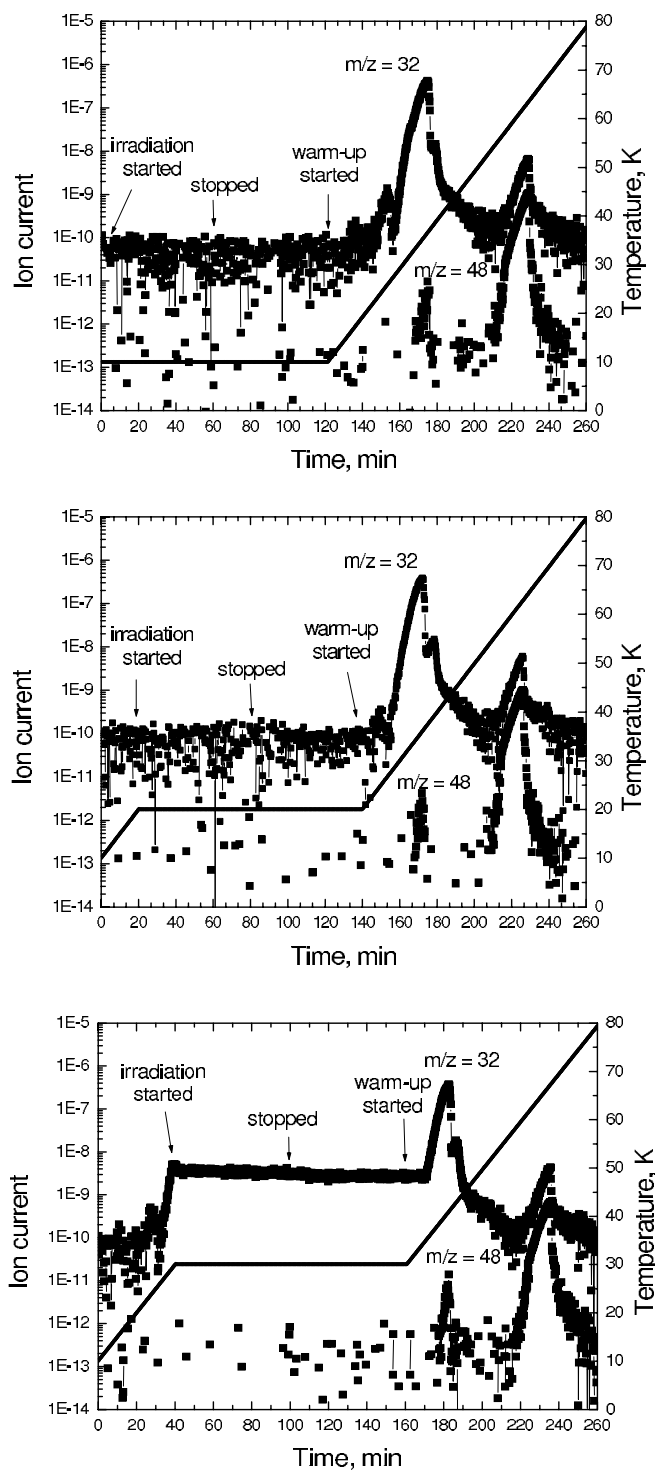
FIG. 4.—Ion current profile of subliming molecular oxygen (O_2), shown in black, and ozone (O_3), shown in gray, monitored via a quadrupole mass spectrometer of the irradiated samples at 11 K (*top*), 20 K (*center*), and 30 K (*bottom*). The solid line indicates the temperature trend. [*See the electronic edition of the Journal for a color version of this figure.*]

out by depositing ozone directly onto a substrate (Chaabouni et al. 2000b). Absorptions of ozone were also observed at $2\nu_3$ (2049 cm^{-1}) and $\nu_2 + \nu_3$ (1725 cm^{-1}) (Fig. 3 and Table 1).

3.2. *Mass Spectrometry*

During the irradiation phase, we did not observe any molecules/ atoms released from the sample into the gas phase. However, as

we started to warm up the irradiated ice, molecular oxygen, monitored via its mass-to-charge (m/z) of 32, was found to sublime at around 25 K, close to the onset of the α-O_2 to β-O_2 phase transition (Fig. 4). The molecular oxygen sublimation plot was found to peak at around 37 ± 2 K. A second peak at $m/z = 32$ was monitored at about 55 K, and this correlates nicely with the temporal evolution of ozone detected via its parent at $m/z = 48$, and therefore, we assign the peak of $m/z = 32$ at $T = 55$ K as originating from dissociative ionization of ozone in the electron impact ionizer of the mass spectrometer, not as being released from the ice. Note that a small peak of $m/z = 48$ was also observable at about 37 K. However, the 37 K peak can be attributed to ion-molecule reactions in the ionizer of the mass spectrometer leading to an ion with $m/z = 48$ and the small amounts of ozone taken away during oxygen desorption.

The complete sublimation of ozone was observed at about 62 K. It should be noted that the observed temperature at which O_3 sublimes depends strongly on the experimental conditions. For instance, β-O_3 can exist until 80 K either in the crystalline form, as a supercooled liquid, or as a metastable state of solid ozone (Hanson & Mauersberger 1986). In our experiments, the sublimation peaks detected by the mass spectrometer for molecular oxygen and ozone fall in the temperature ranges of 37–43 and 62–66 K, respectively.

4. DISCUSSION

4.1. *Irradiation Phase*

Ozone, monitored with the strong ν_3 (1037 cm^{-1}) band, was observed to form immediately upon the onset of irradiation of the oxygen film. This feature can be used to quantify the amount of ozone formed during the irradiation phase, during the isothermal phase, and during the warm-up regime. The column density of the ozone may then be estimated using a modified Lambert-Beer law with an absorption coefficient of the ν_3 fundamental of 1.4×10^{-17} cm molecule^{-1} (Bennett & Kaiser 2005). Based on this ν_3 fundamental, we can extract the temporal evolution of the column density of the ozone molecule. By fitting these data to kinetic rate laws, we can extract rate constants and obtain information on the underlying reaction mechanisms forming ozone at temperatures of 11, 20, and 30 K.

The infrared spectroscopic detection of ozone, O_3, and the accompanying [O_3...O] complex (Fig. 2) suggests that the interaction of the keV electrons with the oxygen molecule leads to a cleavage of the oxygen-oxygen bond forming two oxygen atoms. Figure 5 displays the temporal evolution of the ozone monomer (Fig. 5*a*), of the [O_3...O] complex (Figs. 5*b* and 5*c*), and of the [O_3...O_3] complex (Fig. 5*d*) for an electron current of 100 nA. The ozone monomer column density is seen to increase with irradiation time at all the temperatures 11, 20, and 30 K. However, the ozone monomer column density is highest in ices prepared at the lowest temperature (11 K; Fig. 5*a*). The column densities of the [O_3...O] complex also increases during irradiation, but here the temperature trend is reversed when compared to the ozone monomer; the actual column density of the [O_3...O] complex rises as the temperature of the oxygen matrix is increased (Fig. 5*b*). However, at longer irradiation times (greater than 24 minutes) the [O_3...O] density is observed to come to equilibrium and the [O_3...O_3] complex appears, rising in intensity with increasing electron exposure.

How can these experimental findings be explained? The data suggest the formation of oxygen atoms during the keV electron exposure. Cosby (1993) has shown that energetic electrons impinging on oxygen molecules can produce oxygen atoms in the
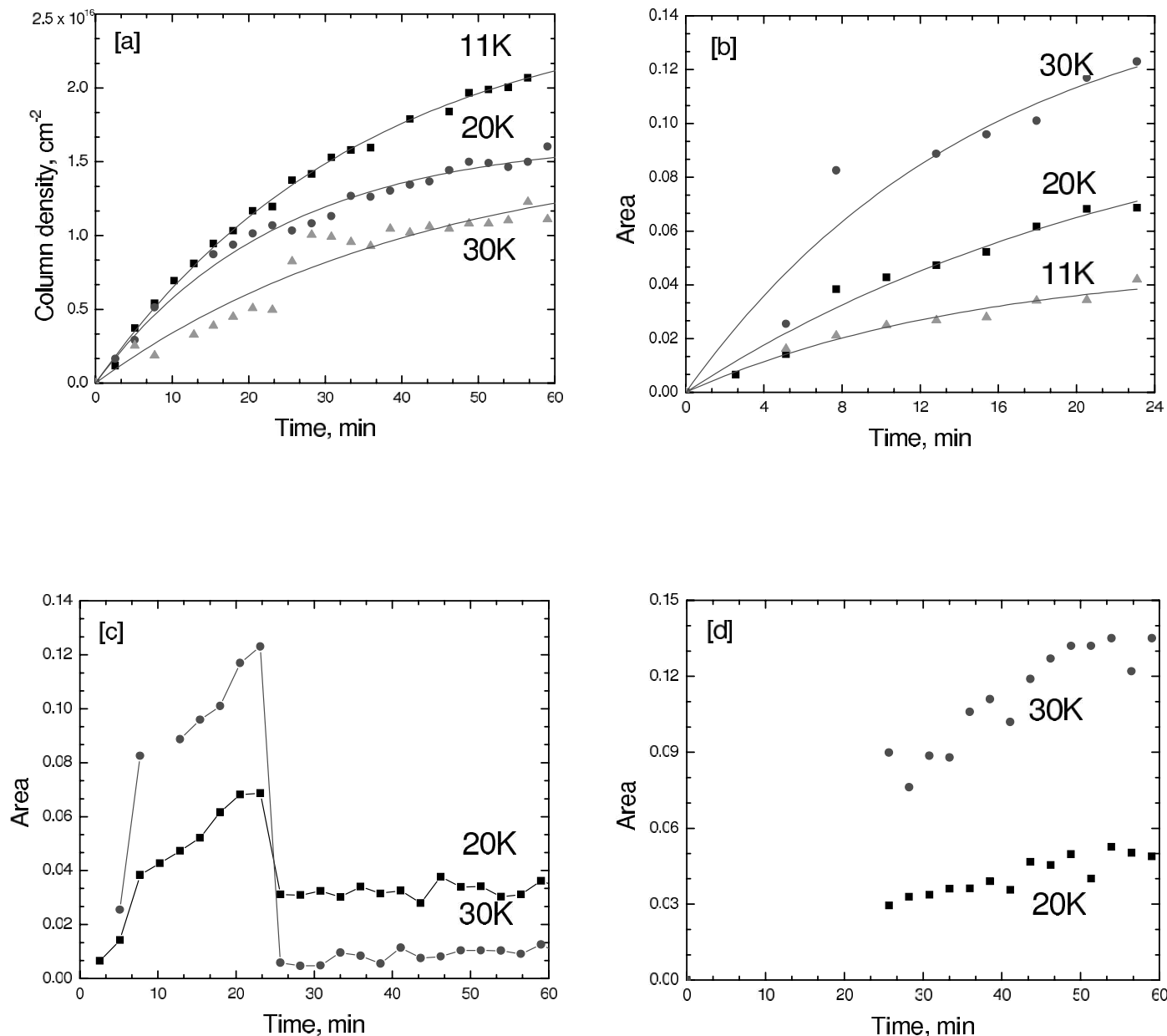
Fig. 5.—(*a*) Temporal growth of the column density of the ozone monomer until the end of the irradiation. (*b*) Temporal growth of the [O$_3$...O] complex during its formation period until 24 minutes into the irradiation. (*c*) Temporal evolution of the [O$_3$...O] complex until the end of the irradiation. (*d*) Temporal growth of the [O$_3$...O$_3$] complex until the end of the irradiation. Error values are within the error limit of $\pm 10\%$ and are not shown for clarity. [*See the electronic edition of the Journal for a color version of this figure.*]

TABLE 2

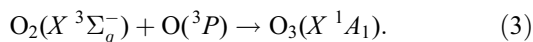Values of the Rate Constants and Pre-exponential Factors for Equation (4)

				O$_3$ Column Density at (cm^{-2})	
Electron Beam Current (nA)	Temperature (K)	k_1 (s^{-1})	a_1 (cm^{-2})	Peak of O$_2$ Sublimation	End of Irradiation
100.............................	11	$(0.48 \pm 0.02) \times 10^{-3}$	$(2.58 \pm 0.05) \times 10^{16}$	$(5.42 \pm 0.27) \times 10^{16}$	$(2.14 \pm 0.22) \times 10^{16}$
	20	$(0.7 \pm 0.04) \times 10^{-3}$	$(1.66 \pm 0.04) \times 10^{16}$	$(5.125 \pm 0.23) \times 10^{16}$	$(1.59 \pm 0.31) \times 10^{16}$
	30	$(0.39 \pm 0.09) \times 10^{-3}$	$(1.60 \pm 0.02) \times 10^{16}$	$(4.32 \pm 0.35) \times 10^{16}$	$(1.18 \pm 0.30) \times 10^{16}$
10.............................	11	$(0.11 \pm 0.05) \times 10^{-3}$	$(2.07 \pm 0.69) \times 10^{16}$	$(2.25 \pm 0.11) \times 10^{16}$	$(7.02 \pm 0.6) \times 10^{15}$
	20	$(0.17 \pm 0.04) \times 10^{-3}$	$(1.28 \pm 0.22) \times 10^{16}$	$(1.79 \pm 0.09) \times 10^{16}$	$(6.14 \pm 0.5) \times 10^{15}$
	30	$(0.07 \pm 0.05) \times 10^{-3}$	$(1.26 \pm 0.49) \times 10^{16}$	$(1.41 \pm 0.13) \times 10^{16}$	$(5.69 \pm 0.37) \times 10^{15}$

TABLE 3
VALUES OF THE RATE CONSTANTS FOR EQUATION (5)

O₃ Complex	Temperature (K)	k_2 (s⁻¹)
O₃...O........................	11	$(1.15 \pm 0.18) \times 10^{-3}$
	20	$(0.68 \pm 0.27) \times 10^{-3}$
	30	$(0.77 \pm 0.24) \times 10^{-3}$

electronic ground (^3P) and in the first electronically excited (^1D) states. At electron energies above 100 eV, the dissociation process of an oxygen molecule produces one oxygen atom in its first electronically excited state (^1D) and a second oxygen atom in its ground state (^3P); a simultaneous production of two ground-state oxygen atoms is less favorable (Cosby 1993). Subsequently, O(^1D) can undergo intersystem crossing (ISC). In an ice matrix, the lifetime of O(^1D) varies strongly from 32 s to 780 ms (Mohammed 1990). We can therefore conclude that after the isothermal phase, all O(^1D) atoms are relaxed to their ^3P ground state. The quenching of O(^1D) to O(^3P) is expected to be a rapid process due to frequent collisions in the solid-state matrix; therefore, the lifetime of electronically excited oxygen atoms is expected to be less than a few μs to 100 ns (Benderskii & Wight 1994; Mohammed 1990; Ning et al. 2000; Turnipseed et al. 1991).

Based on these considerations, we propose the following reaction mechanisms leading to the observed ozone formation. On interaction of the 5 keV electrons with molecular oxygen, two oxygen atoms are formed. During this process, oxygen atoms are formed with high kinetic energies up to a few electron volts. These oxygen atoms are not in thermal equilibrium with the surrounding ice and must be classified as suprathermal (Bennett & Kaiser 2005). If an oxygen atom has enough excess kinetic energy, it can escape its formation site in the lattice to react with a neighboring oxygen molecule forming ozone via equation (3)

$$O_2(X\ ^3\Sigma_g^-) + O(^3P) \rightarrow O_3(X\ ^1A_1). \qquad (3)$$

However, in the limiting case, an oxygen atom can also be formed with no excess kinetic energy so that it is "trapped" in the matrix site. Increasing the temperature from 11 to 30 K means they would gain excess thermal energy. This enhances the mobility of these atoms to migrate. In principle, three reaction pathways are open: (1) the oxygen atoms can react with one another to "recycle" molecular oxygen, (2) oxygen migrates to a neighboring ozone molecule forming a [O₃...O] complex, or (3) the oxygen atom diffuses to an oxygen molecule reacting via equation (3) to form ozone. If pathway 3 dominates, we would expect an increase in ozone concentration, as the temperature rises from 11 to 30 K. This has clearly not been observed experimentally (Fig. 5a), and pathway 3 may be the least preferred reaction pathway for a given oxygen atom. Since, in pathway 1, atomic oxygen would recombine with a neighboring oxygen atom, this would ensure fewer oxygen atoms are available to form ozone via equation (3), and we expect a decreased ozone production as the temperature increases. This is in agreement with the temperature-dependent temporal profile of the ozone monomer (Fig. 5a). Considering the proposed reaction mechanisms, we would expect that the temporal evolution of the column densities of the ozone monomer and of the [O₃...O] complex can be fit by pseudo first-order equations (4) and (5). We would like to stress that the integral absorption coefficient of the [O₃...O] complex is unknown, so we only fit the temporal evo-
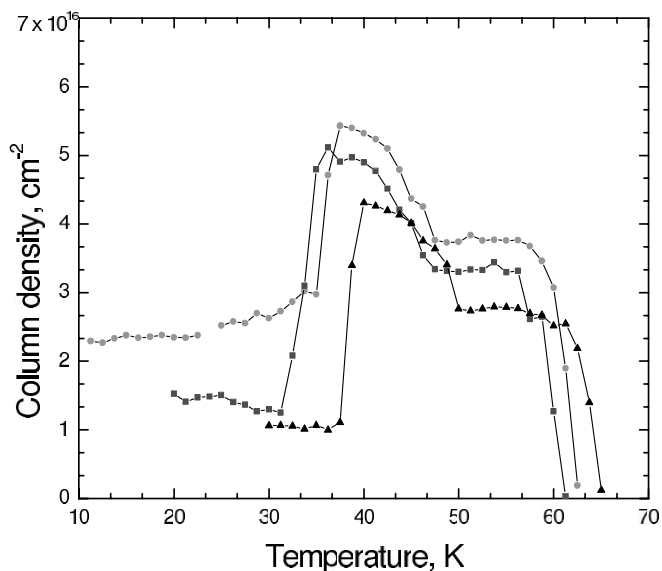

FIG. 6.—Column density of the ν_3 band of ozone monomer during warm-up of the sample at the rate of 0.5 K minute⁻¹ for the samples irradiated at 11, 20, and 30 K at electron beam current of 100 nA. Values are within the error limit of ±10%. Error bars are not shown for clarity. [*See the electronic edition of the Journal for a color version of this figure.*]

lution of the band area. The data are compiled in Tables 2 and 3. It is worth mentioning that the rate constants are within the same order of magnitude of each other; indeed, at 10 nA the rate constants on the formation of the ozone monomer are, within the error limits, identical,

$$[O_3](t) = a_1\left(1 - e^{-k_1 t}\right), \qquad (4)$$

$$[[O_3\ldots O]](t) = a_2\left(1 - e^{-k_2 t}\right). \qquad (5)$$

4.2. *Warm-up Phase*

The warm-up of the sample was started after the isothermal phase at a rate of 0.5 K minute⁻¹. Recall that on the onset of the annealing phase, all oxygen atoms stored in the matrix are expected to be the in their electronic ground state (^3P; § 4.1). In addition, at 11 K atomic oxygen does not diffuse; recent experimental studies suggested lifetimes of O(^3P) atoms in oxygen at these temperatures to be on the order of days (Krueger & Weitz 1992). As the temperature is increased, the [O₃...O] signal decreases. Simultaneously, the absorptions of the O₃ monomers (Fig. 6) and of the [O₃...O₃] complexes rise. Indeed, the dissociation of [O₃...O] and simultaneous formation of [O₃...O₃] complexes are observed as soon as the warm-up phase starts. This suggests that at least some of the oxygen atoms in the [O₃...O] complexes react with a neighboring oxygen molecule to form an [O₃...O₃] complex. It is also worth noting that the column densities of the ozone monomer doubled at temperatures close to the oxygen peak sublimation (Table 2). This indicates that oxygen atoms trapped in the matrix can diffuse and react with molecular oxygen to form ozone. As the temperature increases even further, the phase transition from α (amorphous) to β (crystalline) ozone is observed at 47 K (Fig. 7). At 62 K, no ozone is left on the substrate. Thus, we can identify two temperature-dependent reaction mechanisms to form ozone *in the annealing phase of the ices*: (1) a reaction of oxygen atoms from the [O₃...O] complex and (2) reactions of trapped
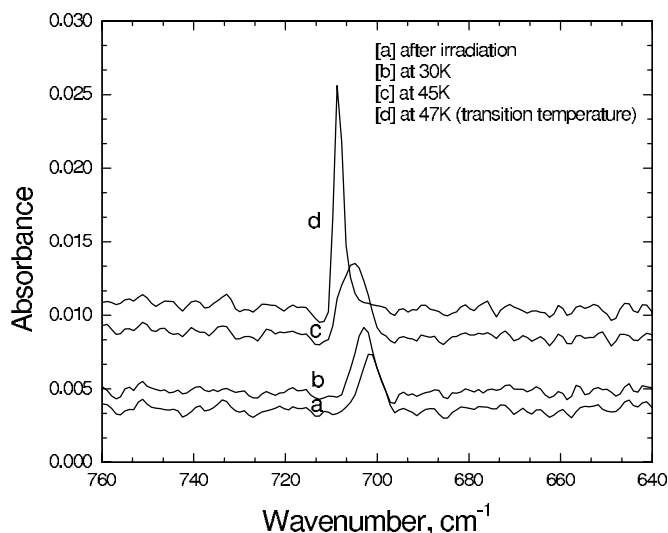
FIG. 7.—The ν_2 fundamental band of O_3 monomer is observed to have shifted by 6.7 cm^{-1}, when the temperature reaches 47 K, thereby indicating phase transition from α to β O_3.

oxygen atoms in the molecular oxygen matrix with oxygen molecules to form ozone.

5. CONCLUSIONS

We have investigated the formation of ozone when solid molecular oxygen at 11, 20, and 30 K is irradiated by 5 keV electrons and the behavior of ozone when warmed to 70 K. Various reaction mechanisms were derived from the experimental data. The amount of ozone formed via electron irradiation is shown to be strongly dependent on the sample temperature, with the ozone monomer column density decreasing as a function of ice temperature between 11 and 30 K. During irradiation, reactions of suprathermal oxygen atoms contribute to a temperature-independent reaction pathway that forms ozone. The loss of oxygen atoms by recombination to "recycle" molecular oxygen is observed to be larger at higher temperatures, hence forming less ozone at elevated temperatures. In the warm-up phase, we identified two additional temperature-dependent reaction mechanisms that synthesize ozone, i.e., a reaction of oxygen atoms from the $[O_3 \ldots O]$ complex with a neighboring oxygen molecule, as demonstrated by the increase in the yield of $[O_3 \ldots O_3]$ complexes, and the reaction of trapped oxygen atoms in the molecular oxygen matrix with oxygen molecules to form the ozone monomer.

These experiments may have profound implications on the oxygen chemistry in icy satellites. Although the laboratory simulations are focused on pure oxygen ices, which have not been observed in our solar system to date, recent experiments suggested that localized concentrations of molecular oxygen may exist in water-rich solar system ices (Zheng et al. 2006). Hence, if sufficient molecular oxygen exists in water ice, ozone can certainly be formed via irradiation with energetic electrons, which in turn, may be formed by magnetospheric ion or solar UV bombardment of the planetary or lunar surfaces.

REFERENCES

Angel, J. R. P., Cheng, A. Y. S., & Woolf, N. J. 1986, Nature, 322, 341
Bahou, M., Schriver-Mazzuoli, L., & Schriver, A. 2001, J. Chem. Phys., 114, 4045
Baragiola, R. A., Atteberry, C. L., Bahr, D. A., & Jakas, M. M. 1999, Nucl. Instrum. Methods Phys. Res. B, 157, 233
Barrett, C. S., Meyer, L., & Wasserma, J. 1967, J. Chem. Phys., 47, 592
Barth, C. A., & Hord, C. W. 1971, Science, 173, 197
Barth, C. A., Hord, C. W., Stewart, A. I., Lane, A. L., Dick, M. L., & Anderson, G. P. 1973, Science, 179, 795
Beichman, C. A., Woolf, N. J., & Lindensmith, C. A. 1999, The Terrestrial Planet Finder (TPF): A NASA Origins Program to Search for Habitable Planets
Benderskii, A. V., & Wight, C. A. 1994, J. Chem. Phys., 101, 292
Bennett, C. J., & Kaiser, R. I. 2005, ApJ, 635, 1362
Berkner, L. V., & Marshall, L. C. 1964, Discussions Faraday Soc., 122
Bertaux, J. L., et al. 2000, Planet. Space Sci., 48, 1303
Brewer, L., & Wang, J. L. 1972, J. Chem. Phys., 56, 759
Brosset, P., Dahoo, R., Gauthierroy, B., Abouafmarguin, L., & Lakhlifi, A. 1993, Chem. Phys., 172, 315
Burke, B. F. 1986, Nature, 322, 340
Cairns, B. R., & Pimentel, G. C. 1965, J. Chem. Phys., 43, 3432
Chaabouni, H., Schriver-Mazzuoli, L., & Schriver, A. 2000a, Low Temp. Phys., 26, 712
———. 2000b, J. Phys. Chem. A, 104, 6962
Chapman, S. 1930, Mem. R. Meteorol. Soc., 3, 103
Cosby, P. C. 1993, J. Chem. Phys., 98, 9560
Dyer, M. J., Bressler, C. G., & Copeland, R. A. 1997, Chem. Phys. Lett., 266, 548
Fama, M., Bahr, D. A., Teolis, B. D., & Baragiola, R. A. 2002, Nucl. Instrum. Methods Phys. Res. B, 193, 775
Freiman, Y. A., & Jodl, H. J. 2004, Phys. Rep., 401, 1
Hanel, R., et al. 1979, Science, 206, 952
———. 1982, Science, 215, 544

Hanson, D., & Mauersberger, K. 1986, J. Chem. Phys., 85, 4669
Hendrix, A. R., Barth, C. A., & Hord, C. W. 1999, J. Geophys. Res. Planets, 104, 14169
Holtom, P. D., Bennett, C. J., Osamura, Y., Mason, N. J., & Kaiser, R. I. 2005, ApJ, 626, 940
Horl, E. M. 1962, Acta Crystallographica, 15, 845
Krueger, H., & Weitz, E. 1992, J. Chem. Phys., 96, 2846
Lacombe, S., Cemic, F., Jacobi, K., Hedhili, M. N., LeCoat, Y., Azria, R., & Tronc, M. 1997, Phys. Rev. Lett., 79, 1146
Leger, A. 2000, Adv. Space Res., 25, 2209
Leger, A., Ollivier, M., Altwegg, K., & Woolf, N. J. 1999, A&A, 341, 304
Leger, A., Pirre, M., & Marceau, F. J. 1994, Ap&SS, 212, 327
Mohammed, H. H. 1990, J. Chem. Phys., 93, 412
Nelson, R. M., Lane, A. L., Matson, D. L., Veeder, G. J., Buratti, B. J., & Tedesco, E. F. 1987, Icarus, 72, 358
Ning, X. J., Zhang, L. N., Chen, M. H., & Qin, Q. Z. 2000, J. Chem. Phys., 112, 386
Noll, K. S., Johnson, R. E., Lane, A. L., Domingue, D. L., & Weaver, H. A. 1996, Science, 273, 341
Noll, K. S., Roush, T. L., Cruikshank, D. P., Johnson, R. E., & Pendleton, Y. J. 1997, Nature, 388, 45
Schrivermazzuoli, L., Desaxce, A., Lugez, C., Camypeyret, C., & Schriver, A. 1995, J. Chem. Phys., 102, 690
Smith, A. L., Keller, W. E., & Johnston, H. L. 1950, Phys. Rev., 79, 728
Spencer, J. R., Tamppari, L. K., Martin, T. Z., & Travis, L. D. 1999, Science, 284, 1514
Teolis, B. D., Loeffler, M. J., Raut, U., Fama, M., & Baragiola, R. A. 2006, ApJ, 644, L141
Turnipseed, A. A., Vaghjiani, G. L., Gierczak, T., Thompson, J. E., & Ravishankara, A. R. 1991, J. Chem. Phys., 95, 3244
Zheng, W. J., Jewitt, D., & Kaiser, R. I. 2006, ApJ, 639, 534